Supporting Material

Tilting and wobble of myosin V by high-speed single molecule polarized fluorescence microscopy

John F. Beausang, Deborah Y. Shroder, Philip C. Nelson and Yale E. Goldman

Choice of Hemisphere

The probe bound to the protein is not symmetrical, due to its specific attachments to the two different Cys residues of the protein. In order to maintain the same end in successive measurements, information is required beyond the individual polarization measurements. If the true rotational motions of the molecule are smaller than 180º, then all of the orientations for one end of the dipole will fall into one hemisphere of orientations. We can find a hemisphere that fulfills this requirement if we assume that all of the measured angles in a processive run are within 90º of the average angle. This assumption is reasonable because the recordings usually contain similar numbers of leading and trailing positions and the total angle change for lever arm of myosin V when it steps is substantially less than 180º as indicated by cryo-electron microscopy (1) and AFM (2).

The polar axis of this molecule-specific hemisphere is inferred from the set of dipole orientations for that molecule. The axis is defined analogous to the director of the nematic liquid crystal order parameter Ξ:

$$\Xi_{i,j} = \frac{1}{n_D}\sum_{k=1}^{n_D}\left(\vartheta_{k,i}\vartheta_{k,j} - \frac{1}{3}\hat{\delta}_{i,j}\right)$$

where n_D is the total number of dwell periods in the recording and $\vec{\vartheta}_k = \langle \sin(\theta_k)\cos(\phi_k),\ \sin(\theta_k)\sin(\phi_k),\ \cos(\theta_k) \rangle$ is the k^{th} orientation of either end of the dipole represented as a unit vector in Cartesian coordinates where i,j =1,2,3 representing the x, y and z directions, and $\hat{\delta}_{i,j}$ is the Kronecker delta function equal to 1 when $i = j$ and zero otherwise. Note that for each angle, regardless of whether $\langle \vartheta_{k,x}, \vartheta_{y,z}, \vartheta_{k,z} \rangle$ or its dipole symmetry related vector $\langle -\vartheta_{k,x}, -\vartheta_{y,z}, -\vartheta_{k,z} \rangle$ is used, Ξ is unchanged. Because Ξ is a 3 × 3 matrix there are 3 orthogonal eigenvectors and the polar axis of the hemisphere is chosen to align with the dominant eigenvector, that is, the eigenvector with the largest eigenvalue.

The end of the director closest to the initial direction of motion of the molecule, as measured from the CCD images recorded prior to the polarization analysis, is chosen as the hemisphere pole for the analysis in the text. The opposite hemisphere corresponds to the molecule walking on the opposite side of the actin filament (3), an experimental detail that is not known for any individual molecule. In any case, the choice of which of these two hemispheres is irrelevant for relative motions during a run.

Supporting References

1. Walker, M. L., S. A. Burgess, J. R. Sellers, F. Wang, J. A. Hammer, J. Trinick, and P. J. Knight. 2000. Two-headed binding of a processive myosin to F-actin. *Nature.* 405(6788): 804-807.

2. Kodera, N., D. Yamamoto, R. Ishikawa, and T. Ando. 2010. Video imaging of walking myosin V by high-speed atomic force microscopy. *Nature*. 468(7320):72-76.

3. Sun, Y and Y. E. Goldman. 2011. Lever-arm mechanics of processive myosins. *Biophys. J.* 101(1):1-11.

Fig. S1

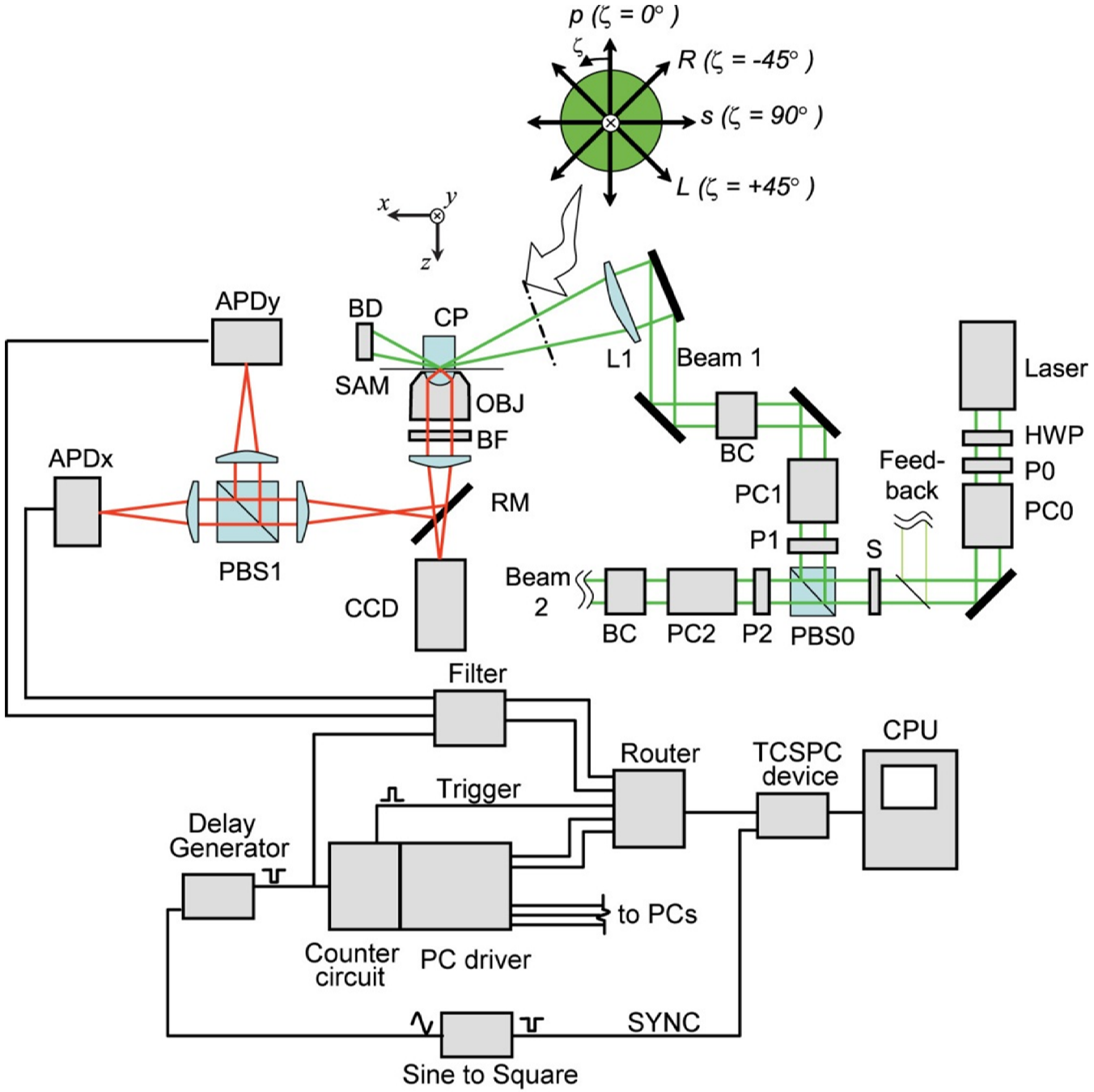
p (ζ = 0°)
R (ζ = -45°)
s (ζ = 90°)
L (ζ = +45°)
ζ
x
y
z
APDy
BD
CP
SAM
OBJ
BF
L1
Beam 1
Laser
HWP
P0
PC0
APDx
RM
BC
PC1
Feed-
back
P1
S
PBS1
CCD
Beam
2
BC
PC2
P2
PBS0
Filter
Router
TCSPC
device
CPU
Trigger
Delay
Generator
to PCs
Counter
circuit
PC driver
SYNC
Sine to Square

Fig. S1. polTIRF setup. The optics of the polTIRF setup have previously been reported (28, 29) and are unchanged other than increasing the rates of polarization switching. Briefly, a 532 nm laser is passed through a Pockels cell (PC0) and split by a polarizing beam splitting cube (PBS0) into two paths, each of which pass through a 2nd Pockels cell (PC1 and PC2) and a Berek compensator (BC1 and BC2), and is then directed by mirrors into a coupling prism at a glancing angle for TIRF illumination. Rapidly cycling the high voltage on the Pockels cells results in four linear input laser polarizations per beam oriented at 0°, ±45°, and 90° for *p*, *L/R*, and *s* polarizations (*inset*). Fluorescence emission from single BR-CaM labeled myosin molecules is collected by the objective, passed through a filter and directed onto a CCD camera. A molecule translocating along actin (Alexa-647 labeled and imaged by a separate 633 nm laser, not shown) is selected for polarization analysis using custom LabView software. The candidate molecule is centered in the image plane by a piezoelectric stage (not shown) and a removable mirror (RM) is rotated into position which directs the polarized fluorescence emission through a beam splitting cube (PBS1) and onto two single photon counting avalanche photodiodes (APDs). Electrical pulses representing each photon are through a router (Becker and Hickl HRT-82) that has been modified to tag each photon with the polarization state of the input laser. The arrival time of these pulses relative to an initial trigger pulse are then precisely measured using a time correlated single photon counting device (TCSPC, Becker and Hickl, SPC-130). A 10 MHz oscillator from the delay generator, synchronizes the Pockels cell drivers and the TCSPC device. More details can be found in reference (50) of the main text.

Fig.S2

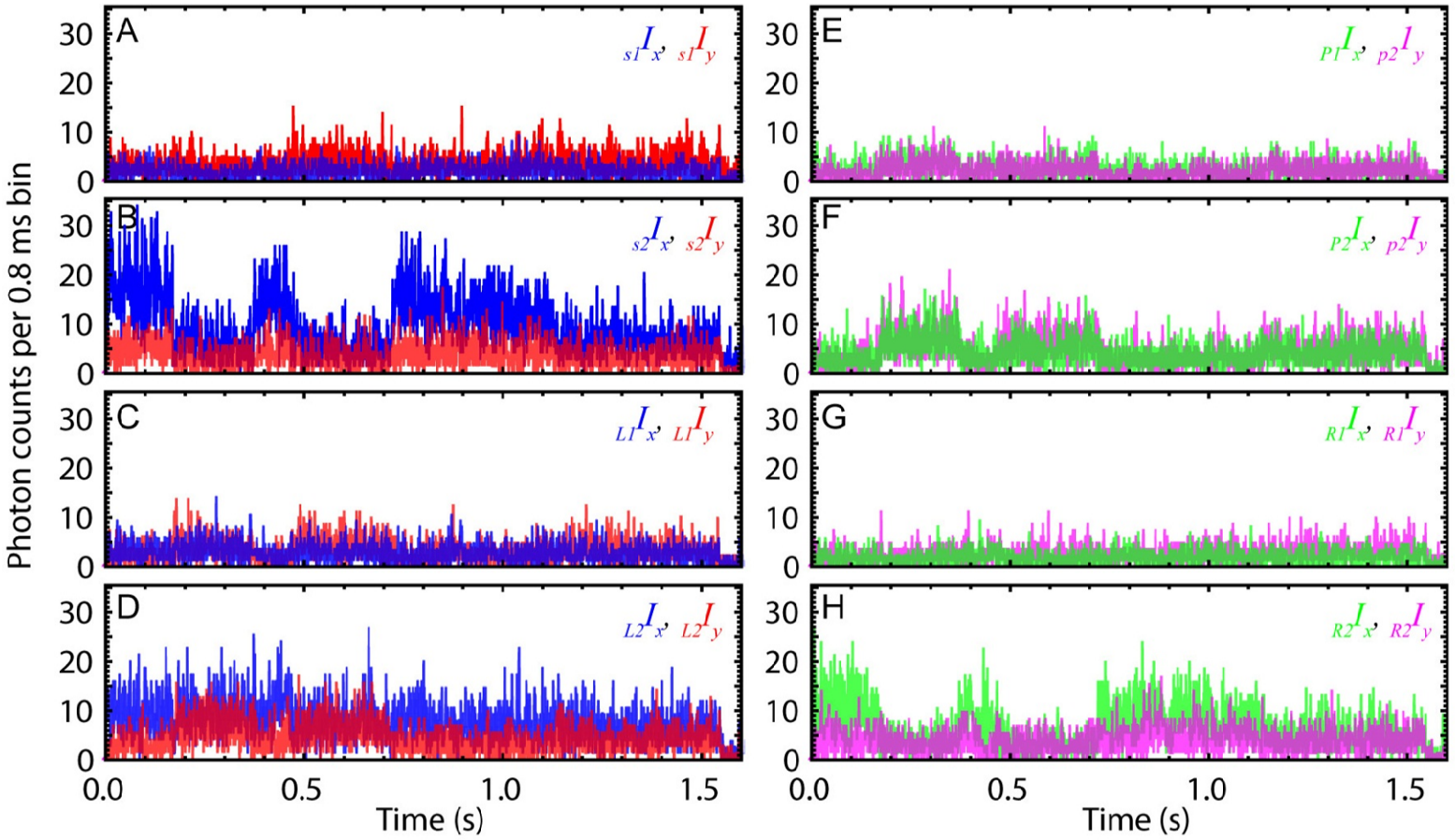

Fig. S2. Data binned at 0.8 ms. Photons are binned within each 0.8 ms cycle of laser polarizations resulting in 16 polarized fluorescence intensities that have a 10x faster time resolution but, consequently, an increase in photon shot noise compared to Fig. 1 of the main text.

Fig. S3

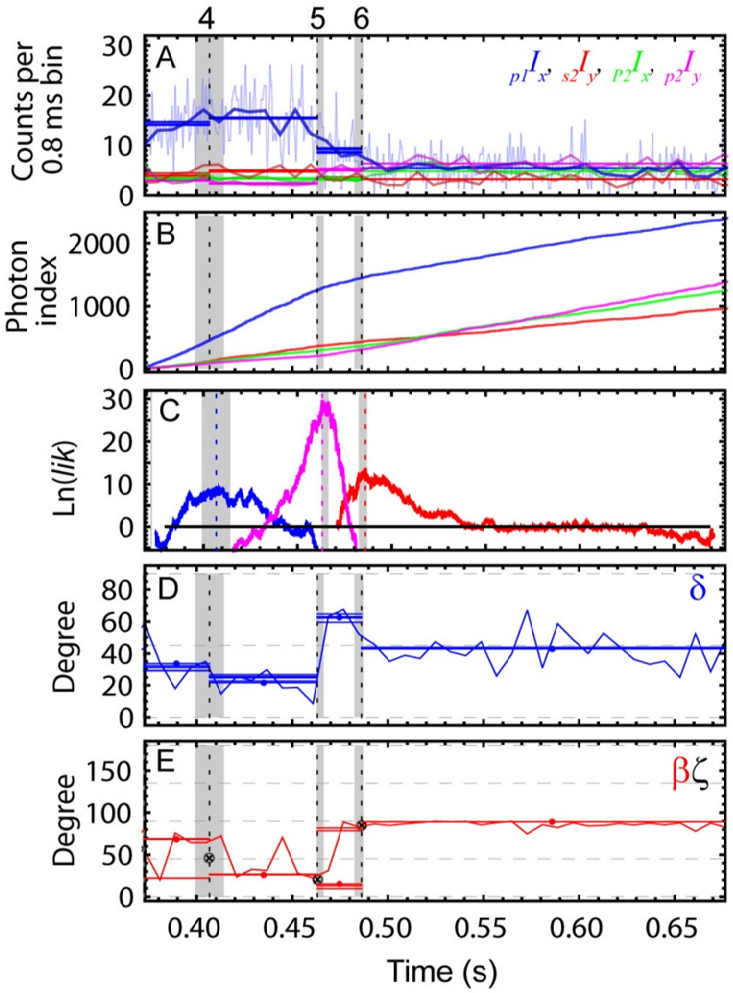

Fig. S3. Detailed analysis of change points. (A) 4 of the 16 PFIs binned at 0.8 ms (*light jagged lines*), averaged over 10 cycles (*dark jagged lines*), and averaged between the change points (*horizontal lines*) demonstrate the altered intensities between change points were detected by the algorithm using the single photon data. (B) The change point algorithm uses the raw photon arrival times, represented here as accumulated photon counts in the same four channels as in (A). Slopes change abruptly at the change points. See Fig. S7 for all 16 traces. (C) The likelihood (*jagged colored lines*) of intensity change points are calculated for each photon in an interval (Materials & Methods). If the peak exceeds the threshold for significance (*black horizontal line* at zero), then its time is the most likely change point (*vertical dashed lines*). 95% confidence intervals (*gray areas behind vertical dashed lines*) are defined as the region where the likelihood curve exceeds the peak value minus two natural log units. (D) Polar angle β and (E) wobble δ were determined using the dipole model for the PFIs binned at 8.0 ms (*jagged lines*) and averaged between change points (5 *horizontal lines, see Materials & Methods for details*). Probe wobble increases between change points #5 and #6 when β changes from ~25° to ~90°.

Fig. S4

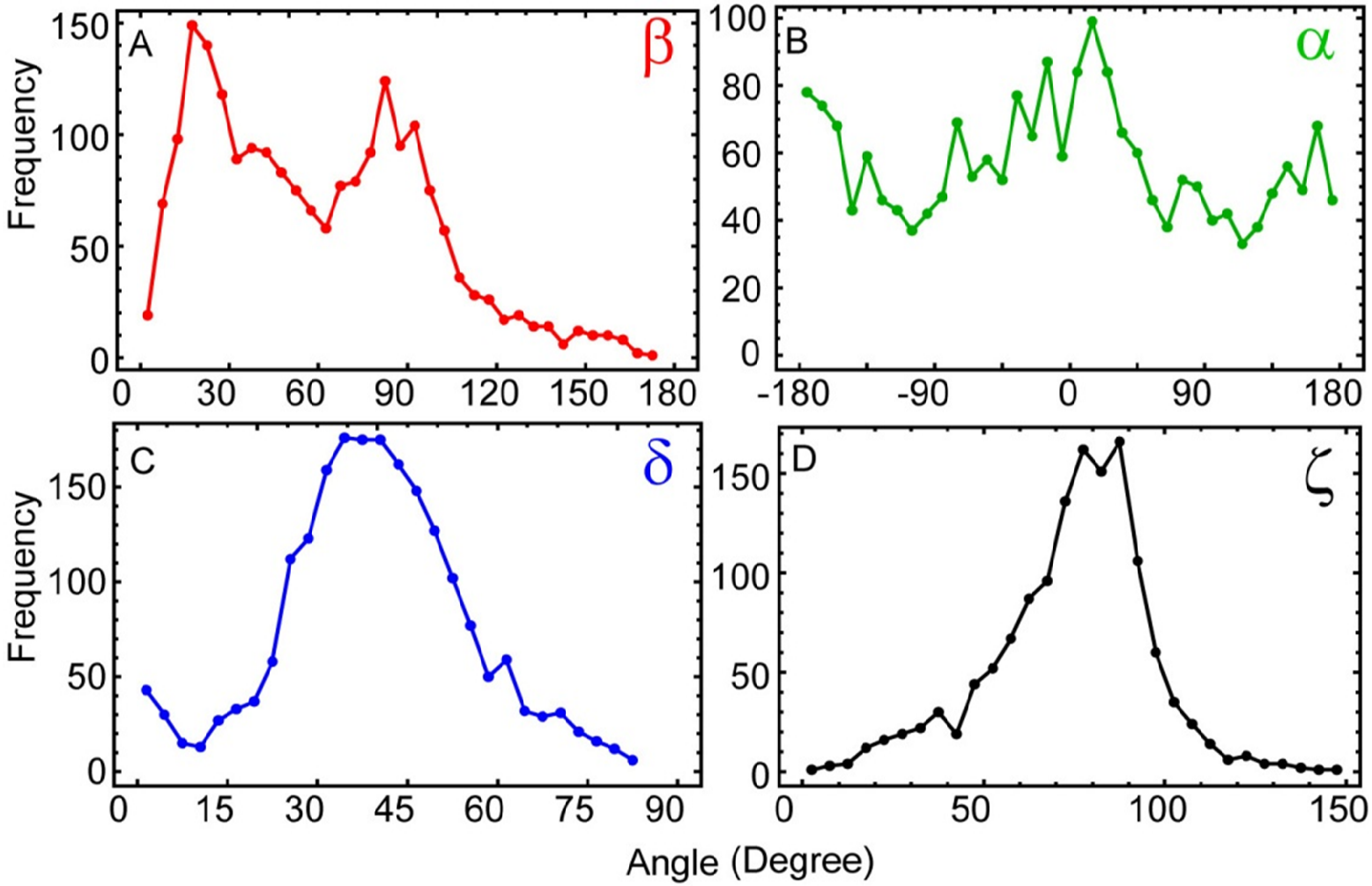

Fig. S4. Distributions of the probe angles. (A) The distribution of the polar angle β has two peaks at 21°±2° and 84°±4° (mode ± S.E. by bootstrapping), due predominately to the trailing and leading configurations of the lever arm, respectively. (B) The distribution of α is approximately uniform with a slight prevalence for the probe to be aligned parallel to the sample plane (α = 0° or 180°). This is consistent with the azimuthal freedom due to the molecule landing at random actin subunits. (C) The distribution of wobble is centered at 39°± 0.4°, which is characteristic of myosin during a two-head bound dwell state. A small tail extending to 90° includes both the high-wobble states of detached heads and the high-wobble state that occurs in some molecules immediately prior to photo-bleaching. (D) Combining $\Delta\beta$ and $\Delta\alpha$ for each step into a single total angle change (ζ, see text for details), results in a distribution that is peaked at $\zeta \approx 80°$.

Fig. S5

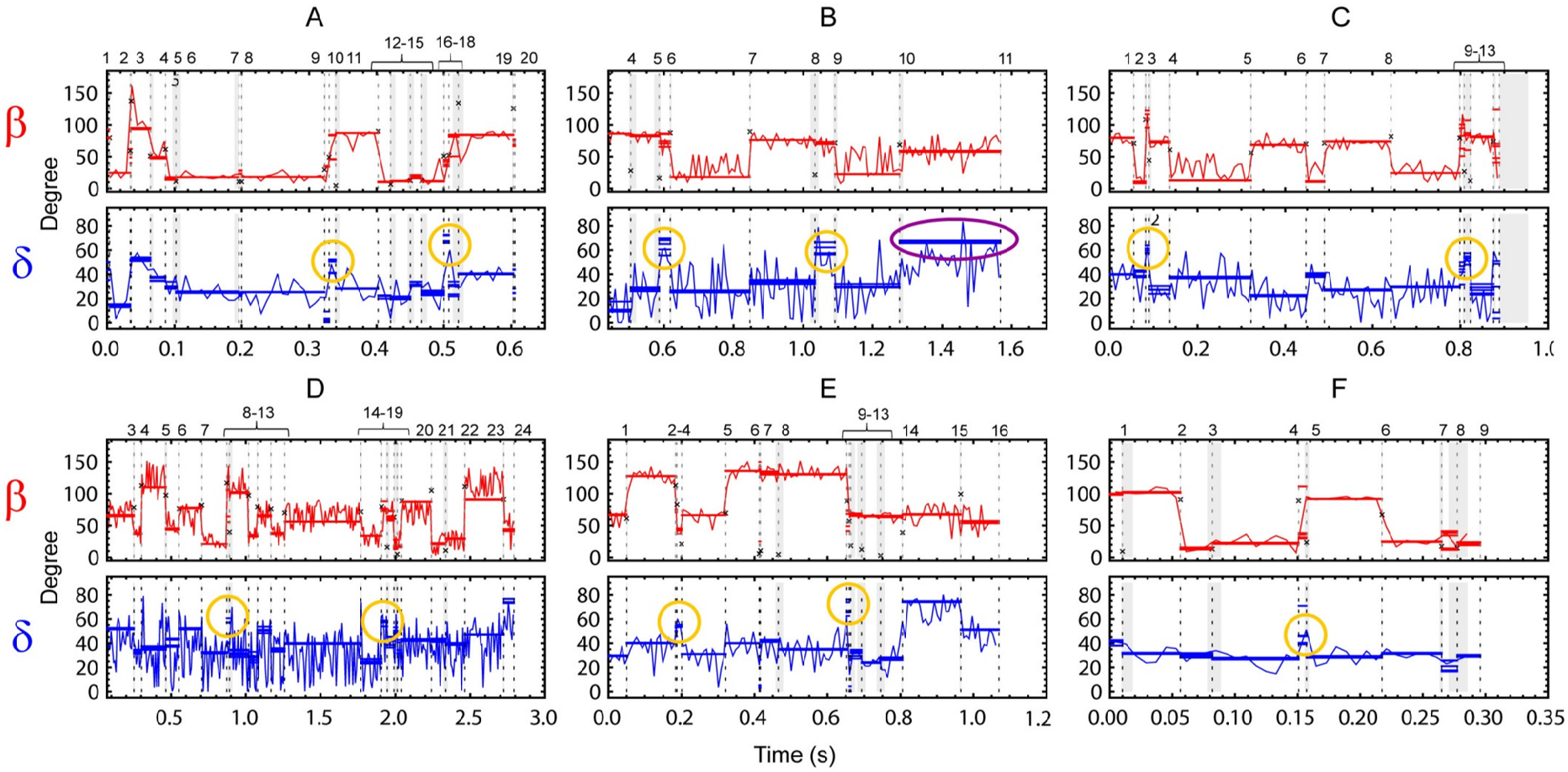

Fig. S5. Gallery of molecules with at least one high-wobble state detected during stepping. (A)-(F) β and δ for 6 molecules showing short-lived increases in δ (*yellow circles*) during stepping (abrupt changes in β, *red*). Molecules with multiple events (A-E) are consistent with the hand-over-hand model of processivity in which the wobble increases every other step (see also Fig. 2E). In 5 out of 6 molecules (A,C-F) the increase in wobble during stepping follows states with low β values, indicating that the trailing head is usually associated with smaller values of β (see also Fig. 3B of the main text). Periods of high wobble sometimes occur prior to photo-bleaching (*purple oval*).

Fig. S6

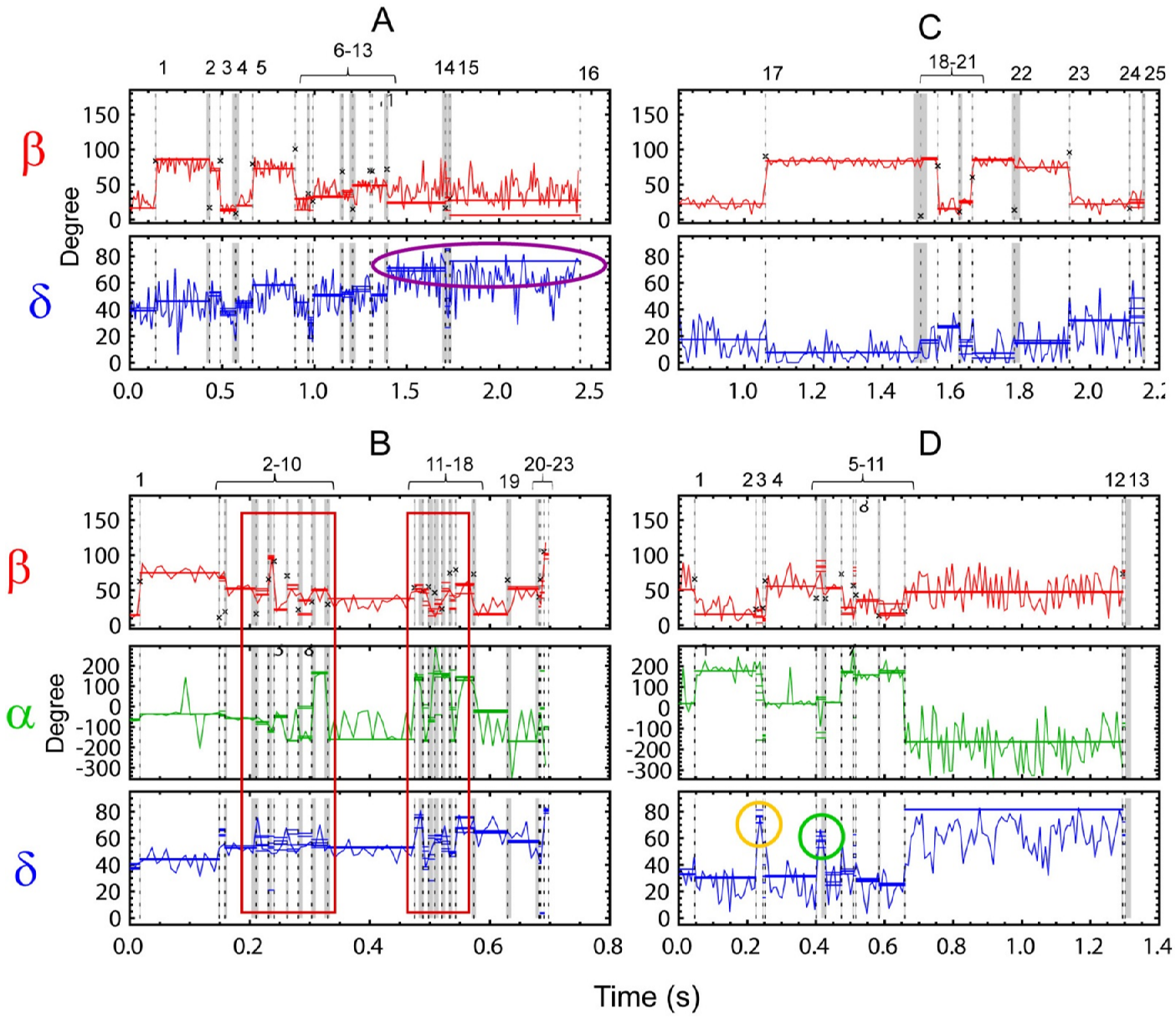

Fig. S6. Gallery of molecules illustrating other types of angular changes. (A) A molecule with increased wobble prior to photo-bleaching (*purple oval*). (B) Rapid polarization changes likely represent a photo-physical effect (red boxes). (C) Some molecules with robust tilting did not always show increases in probe wobble during stepping. (D) Increases in wobble typically occur during a change in β (*orange circles*) but similar states were sometimes observed without changes in β (*green circles*) and may represent non-step angles changes, such as 'foot stomps' or test steps.

Fig. S7

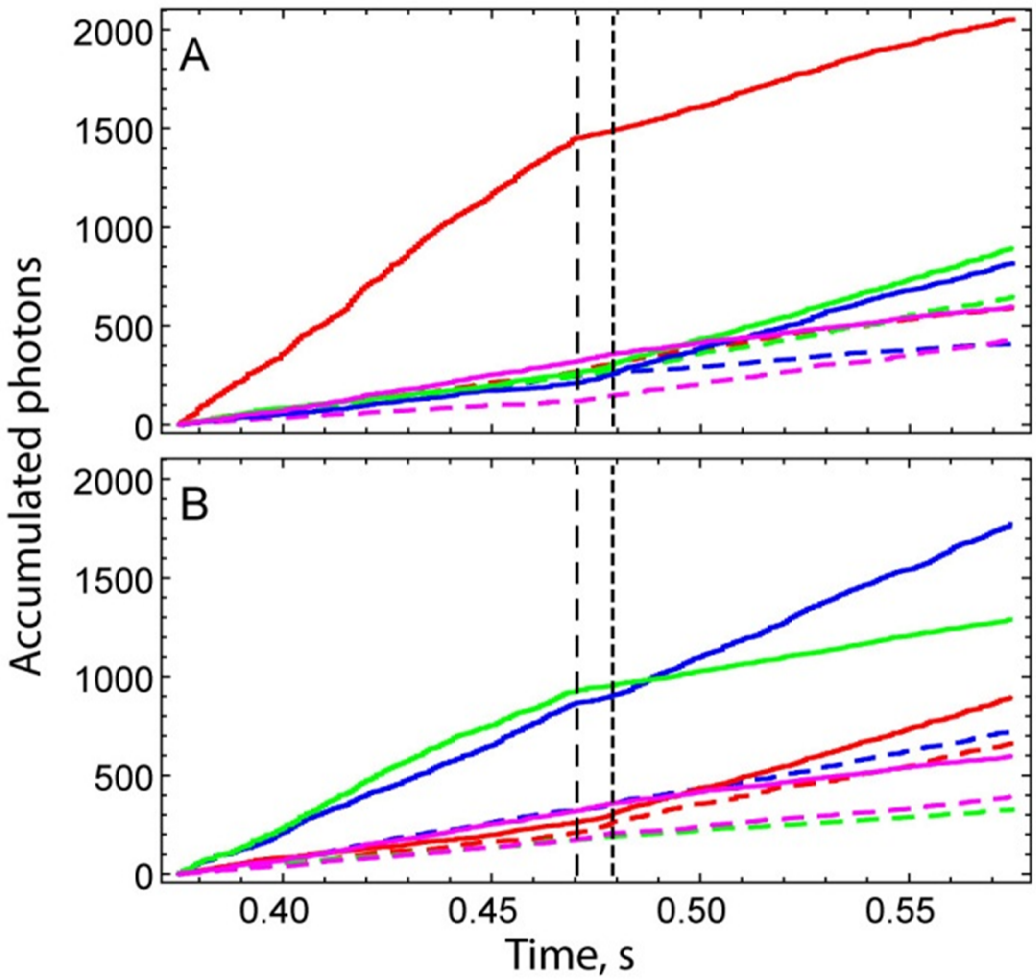

Fig. S7. Single photon traces for all 16 PFIs for the interval shown in Fig. S3. Instead of binning the single photon data, plotting the accumulated number of photons in each polarized fluorescence channel (colors are the same as in Fig. 1 and Fig. S3A) against each photon's arrival time for APDx (*solid lines*) and APDy (*dashed lines*) results in traces that represent constant intensity as constant slope. A change in intensity causes a kink (a sudden change in slope).

Fig. S8

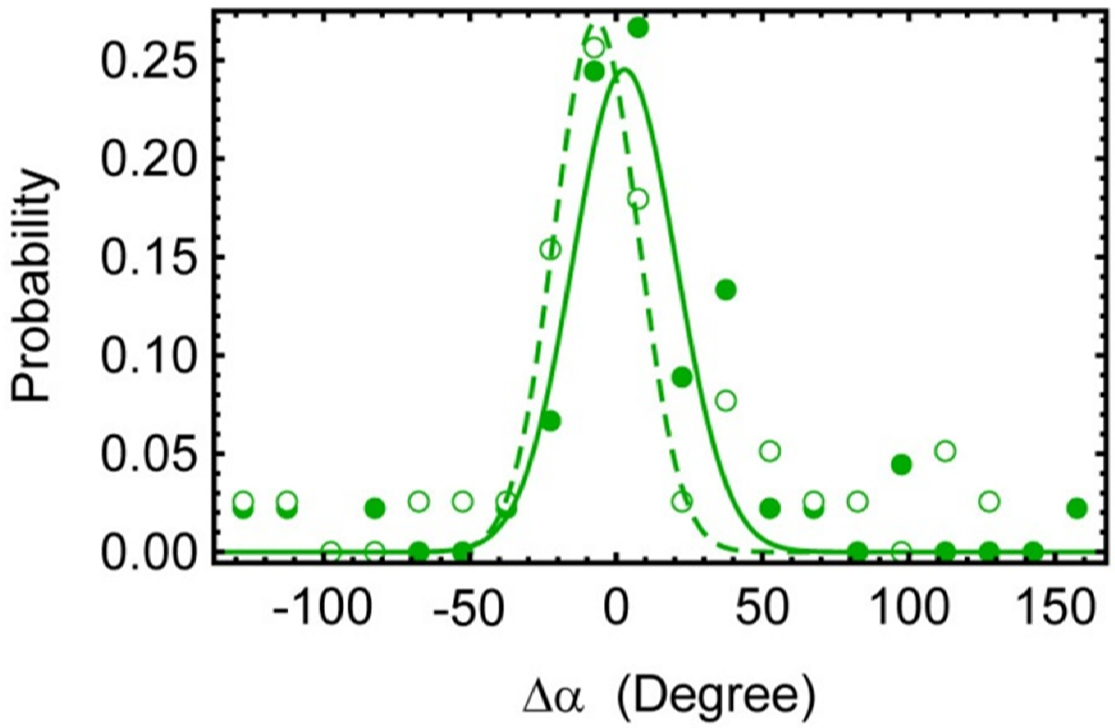

Fig. S8. Distributions of non-step α angle changes (n=73) As in Fig. 5, using only molecules with steps exhibiting a high-wobble state during stepping were included so that the dwells could be unambiguously assigned to the trailing (*filled circles*) and leading heads (*open circles*). Gaussian curves fitted to the distribution of $\Delta\alpha$ changes on the trailing (*solid lines*) and leading heads (*dashed lines*) are similar. The corresponding plot for $\Delta\beta$ is shown in Fig. 5B.